Deterministic interconversions between the Greenberger-Horne-Zeilinger states and the *W* states by invariant-based pulse design

Ri-Hua Zheng,[1,2] Yi-Hao Kang,[1,2] Du Ran,[1,2,3] Zhi-Cheng Shi,[1,2] and Yan Xia[1,2,*]

[1]*Department of Physics, Fuzhou University, Fuzhou 350116, China*

[2]*Fujian Key Laboratory of Quantum Information and Quantum Optics (Fuzhou University), Fuzhou 350116, China*

[3]*Department of Electrical Engineering Physical Electronics, Tel Aviv University, Ramat Aviv 69978, Israel*

(Received 28 October 2019; published 28 January 2020)

In the paper, we propose a protocol for the one-step interconversions between the Greenberger-Horne-Zeilinger (GHZ) states and the *W* states with deterministic success probabilities. The Rydberg interactions among three Rydberg atoms are utilized here to structure nonlocal operations for the interconversions. Additionally, we construct a Lewis-Riesenfeld invariant for a four-level system and afterwards use it to reversely design the Rabi frequencies of the effective Hamiltonian. The numerical simulations indicate that the protocol is robust against the spontaneous emission, the dephasing, the thermal noise, the systematic errors on Rabi frequencies, and the frequency mismatching. Therefore, the protocol may contribute to the research of the interconversions between entanglements.

DOI: 10.1103/PhysRevA.101.012345

I. INTRODUCTION

It is known that quantum entanglement plays an indispensable role in the application of quantum information processing (QIP) [1–4]. Among different entangled states, three-particle entangled states like the Greenberger-Horne-Zeilinger (GHZ) states $[|\mathrm{GHZ}\rangle = (|000\rangle + |111\rangle)/\sqrt{2}]$ and the *W* states $[|W\rangle = (|001\rangle + |010\rangle + |100\rangle)/\sqrt{3}]$ have attracted many interests. With the development of research, scientists found that both the GHZ states and *W* states can be used to test quantum mechanics against local hidden theory without Bell inequality [5–7]. On the other hand, the GHZ states and *W* states possess their own characteristics. For example, a *W* state is robust against the loss of a particle: when one of the three particles loses, the other two particles may still be entangled [8]. Besides, a GHZ state will collapse into a mixed state with only classical correlations if any one of the three particles is lost. Since the GHZ states and *W* states own large information capacity, they are widely used in many practical fields, for example, quantum teleportation [9–12], quantum secure direct communication [13,14], quantum state sharing [15,16], and so on.

As is well known, the GHZ states and the *W* states are two different types of entangled states, and their interconversions cannot be implemented only with local operations and classical communication (LOCC) [8]. However, with the GHZ states and *W* states being widely used in various kinds of QIP, researchers cannot help but think, if one can carry on flexible interconversions between them, the GHZ states or the *W* states will be regarded as the universal 3-qubit entanglements resources. Obviously, it will improve the efficiency of some QIP needing the GHZ states and *W* states. For this purpose, in 2005, Walther *et al.* [17] proposed a conversion of a GHZ state to an approximate *W* state by exploiting the local positive operator valued measures (POVMs) and experimentally applied the protocol in a three-photon system. The protocol provided an innovative method to overcome the difficulty for converting a GHZ state into a *W* state. Nevertheless, the conversion in Ref. [17] is probabilistic because it is indispensable to set imperfect local POVMs, which means the success probability is inversely proportional to the fidelity. In a long period after that, some outstanding protocols have been put forward to solve the problem about the conversions of entangled states, such as the transformation of two Einstein-Podolsky-Rosen (EPR) photon pairs into a *W* state [18] and the conversion of a cluster state into a GHZ state or a Dicke state [19]. But the question about the conversions between the GHZ states and the *W* states is still challenging. In order to get the question settled, Cui *et al.* [20] proposed a protocol for converting a four-photon GHZ state to a *W* state with high fidelity based on homodyne measurement in an optical system. In addition, Kang *et al.* [21] put forward a protocol to realize interconversions between the GHZ states and the *W* states in a spin system. References [20,21] successfully solved the problem of the conversions between the GHZ states and the *W* states in an optical system and a spin system, respectively. However, there are few works focusing on the conversions in an atomic system.

An atom is a type of useful information carrier because it can store the information in stationary nodes. This characteristic makes the atomic system popular for use in many different kinds of QIP [22–33]. Naturally, the conversions between the GHZ states and the *W* states in an atomic system become meaningful. For realizing the conversions, Song *et al.* [34] creatively designed a way to convert a *W* state into a GHZ state with high fidelity based on dissipative dynamics processes. Also, Wang *et al.* [35] proposed a method for the transformation from a *W* state to a GHZ state in spatially separated cavities with 100% fidelity and maximal 75% success

*xia-208@163.com

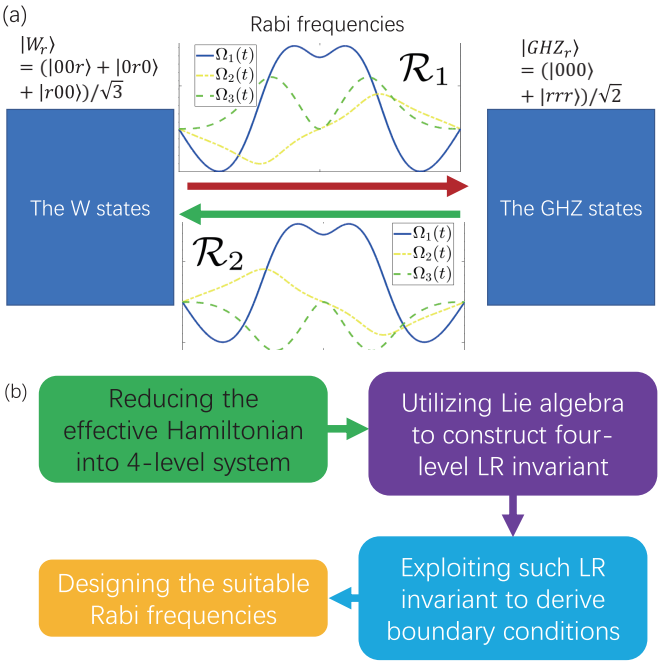

FIG. 1. (a) Schematic diagram of the protocol. In atomic systems, three stationary qubits, initially encoded on the W states, can be transferred (by one step) to the GHZ states with a sequence of Rabi frequencies indicated by $\mathcal{R}_1$, vice versa, the GHZ states can be converted (by one step) into the W states with $\mathcal{R}_2$, a sequence of another Rabi frequencies. (b) Detailed processes for designing the suitable Rabi frequencies $\mathcal{R}_1$ and $\mathcal{R}_2$. "LR invariant" represents the Lewis-Riesenfeld invariant.

probability. Both protocols [34,35] created an irreversible way from a W state to a GHZ state, which means the applications of protocols [34,35] may be limited in some situations where transformations from GHZ states to W states are needful.

In order to work out the unresolved problem regarding interconversions between GHZ states and W states in an atomic system, we propose a protocol utilizing Rydberg interactions [36–39] to structure nonlocal operations for the interconversions. A schematic diagram for the protocol is given in Fig. 1(a), where $\mathcal{R}_1$ represents the sequence of Rabi frequencies for converting the W states into the GHZ states, and $\mathcal{R}_2$ indicates the sequence of Rabi frequencies for transforming the W states to GHZ states. Also, detailed processes for designing suitable Rabi frequencies are shown in Fig. 1(b). The physical model of the protocol contains three neutral atoms with Rydberg states, and each atom is driven by four laser pulses. The original Hamiltonian of the physical system can be refined as a four-level effective Hamiltonian with three time-dependent Rabi frequencies of laser pulses. In order to design suitable Rabi frequencies of the effective Hamiltonian for the interconversions, we exploit Lie algebra [40] to build a Lewis-Riesenfeld (LR) invariant [41]. Moreover, based on the LR invariant, we can inversely design the three time-dependent Rabi frequencies of pulses for the interconversions.

In this paper, we also give numerical simulations for the fidelities of the interconversions by using the original Hamiltonian. The results show that both the conversions from the GHZ states to the W states and conversions from the W states to the GHZ states are stable against the influence of spontaneous emission, dephasing, thermal noise, systematic errors, and frequency mismatching. Therefore, the protocol is feasible in experiment and might be helpful for conversions between entanglements in an atomic system.

The article is organized as follows. In Sec. II, we utilize the Rydberg interactions among three Rydberg atoms to structure nonlocal operations. After calculating, we can derive a four-level effective Hamiltonian. In Sec. III, based on the LR invariant and Lie algebra, we inversely design the Rabi frequencies of laser pulses for the four-level effective Hamiltonian to realize the interconversions between the GHZ states and the W states. Next, we give the numerical simulations in Sec. IV, the expansion of model in Sec. V, and the conclusion in Sec. VI.

II. PHYSICAL MODEL TO REALIZE THE INTERCONVERSIONS BETWEEN THE GHZ STATES AND THE W STATES

We consider a physical system containing three neutral atoms with Rydberg states. As shown in Fig. 2, each particle has one ground state $|0\rangle_k$ $(k = 1, 2, 3)$ and one Rydberg state $|r\rangle_k$, where k denotes the kth atom in the physical system. The transition $|0\rangle_k \leftrightarrow |r\rangle_k$ is driven by four different classical fields with Rabi frequencies $\Omega_{r1}(t)$, $\Omega_{r2}(t)$, $\Omega_{r3}(t)$, and Ω_{r4}, whose detunings are δ_1, $\Delta_2 + \delta_2$, $\Delta_3 + \delta_3$, and Δ_4, respectively. Here, Rabi frequencies $\Omega_{r1}(t)$, $\Omega_{r2}(t)$, and $\Omega_{r3}(t)$ are time dependent and Ω_{r4} is time independent. Each two adjacent atoms have Rydberg interaction with interaction energy V. In the interaction picture, the Hamiltonian is $(p, q, k = 1, 2, 3)$

$$\begin{aligned} H(t) = \sum_{k=1}^{3} [&\Omega_{r1}(t)e^{-i\delta_1 t} + \Omega_{r2}(t)e^{-i(\delta_2+\Delta_2)t} \\ &+ \Omega_{r3}(t)e^{-i(\delta_3+\Delta_3)t} + \Omega_{r4}e^{i\Delta_4 t}]|r\rangle_k\langle 0| \\ &+ \text{H.c.} + \sum_{p<q} V|rr\rangle_{pq}\langle rr|. \end{aligned} \tag{1}$$

Here, the conditions $\Delta_2 = V$, $\Delta_3 = 2V$ and $\{V, \Delta_4\} \gg \{\Omega_{r4}, \delta_1, \delta_2, \delta_3\} \gg \max\{|\Omega_{r1}(t)|, |\Omega_{r2}(t)|, |\Omega_{r3}(t)|\}$ are set. The effective Hamiltonian will be finally derived as (see Appendix for the detailed processes)

$$\begin{aligned} H_{\text{eff}}(t) = &\sqrt{3}\Omega_{r1}(t)|000\rangle\langle W_r| + \sqrt{3}\Omega_{r3}(t)|W_r'\rangle\langle rrr| \\ &+ 2\Omega_{r2}(t)|W_r\rangle\langle W_r'| + \text{H.c.}, \end{aligned} \tag{2}$$

with choosing

$$\begin{aligned} \lambda_1 &= -\frac{6\Omega_{r4}^2}{\Delta_4} + \frac{4\Omega_{r4}^2}{\Delta_4 + V}, \quad \lambda_2 = \frac{4\Omega_{r4}^2}{\Delta_4 + V} - \frac{6\Omega_{r4}^2}{\Delta_4 + 2V}, \\ \lambda_3 &= -\frac{2\Omega_{r4}^2}{\Delta_4 + V}, \quad \lambda_4 = \frac{3\Omega_{r4}^2}{\Delta_4} - \frac{8\Omega_{r4}^2}{\Delta_4 + V} + \frac{3\Omega_{r4}^2}{\Delta_4 + 2V}. \end{aligned} \tag{3}$$

Note that here we code the logical 0 at ground state $|0\rangle$ and the logical 1 at Rydberg state $|r\rangle$, that is, $|W_r\rangle$ $[|W_r\rangle = (|00r\rangle + |0r0\rangle + |r00\rangle)/\sqrt{3}]$ represents the W states and

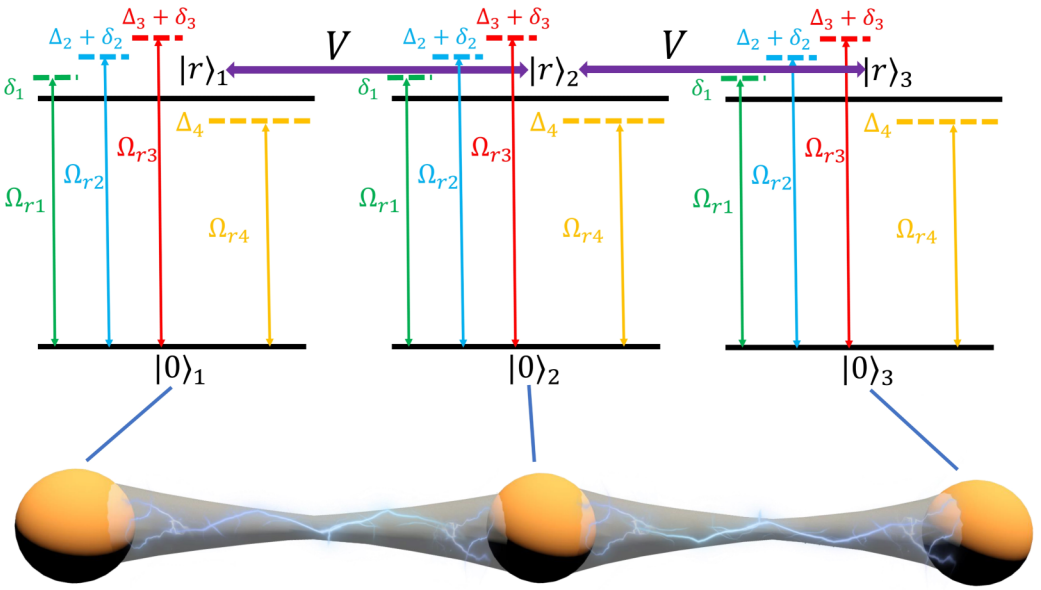

FIG. 2. The energy levels of the three neutral atoms with Rydberg states.

naturally the GHZ states can be defined as

$$|\mathrm{GHZ}_r\rangle = (|000\rangle + |rrr\rangle)/\sqrt{2}. \tag{4}$$

In the following work, the interconversion we want to process is between $|W_r\rangle$ and $|\mathrm{GHZ}_r\rangle$.

III. PULSE DESIGN FOR THE INTERCONVERSIONS VIA INVARIANT

As shown in Eq. (2), the effective Hamiltonian is four level. Hence, in this part, a method for designing Rabi frequencies of such four-level effective Hamiltonians to implement the interconversions between the GHZ states and the W states is given. First of all, we briefly describe the LR theory [41] by introducing a Hermitian invariant operator $I(t)$, which satisfies ($\hbar = 1$)

$$i\frac{\partial I(t)}{\partial t} - [H_{\mathrm{eff}}(t), I(t)] = 0. \tag{5}$$

According to the theory, a solution $|\Psi(t)\rangle$ of the time-dependent Schrödinger equation $i\partial|\psi(t)\rangle/\partial t = H_{\mathrm{eff}}(t)|\psi(t)\rangle$ can be described by the eigenvectors $|\Phi_n(t)\rangle$ ($n = 1, 2, 3, 4$) of $I(t)$ as

$$|\Psi(t)\rangle = \sum_n C_n e^{i\alpha_n}|\Phi_n(t)\rangle, \tag{6}$$

where α_n is the LR phase written as

$$\alpha_n(t) = \int_0^t \langle\Phi_n(t')|\left[i\frac{\partial}{\partial t'} - H_{\mathrm{eff}}(t')\right]|\Phi_n(t')\rangle dt', \tag{7}$$

and

$$C_n = \langle\Phi_n(0)|\Psi(0)\rangle. \tag{8}$$

Next, we build the LR invariant with Lie algebra in a four-level system whose basis is $\{-i|000\rangle, |W_r\rangle, |W_r'\rangle, |rrr\rangle\}$.

In such a basis, Eq. (2) can be rewritten as

$$H_{\mathrm{eff}}(t) = \begin{pmatrix} 0 & \Omega_1(t) & 0 & 0 \\ \Omega_1(t) & 0 & \Omega_2(t) & 0 \\ 0 & \Omega_2(t) & 0 & \Omega_3(t) \\ 0 & 0 & \Omega_3(t) & 0 \end{pmatrix}, \tag{9}$$

with $\Omega_1(t) = i\sqrt{3}\Omega_{r1}(t)$, $\Omega_2(t) = 2\Omega_{r2}(t)$, and $\Omega_3(t) = \sqrt{3}\Omega_{r3}(t)$ [$\Omega_1(t)$, $\Omega_2(t)$, and $\Omega_3(t)$ always being real]. Then $H_{\mathrm{eff}}(t)$ can be resolved as

$$H_{\mathrm{eff}}(t) = \Omega_1(t)G_1 + \Omega_2(t)G_2 + \Omega_3(t)G_3, \tag{10}$$

where G_1, G_2, and G_3 are

$$G_1 = \begin{pmatrix} 0 & 1 & 0 & 0 \\ 1 & 0 & 0 & 0 \\ 0 & 0 & 0 & 0 \\ 0 & 0 & 0 & 0 \end{pmatrix}, \quad G_2 = \begin{pmatrix} 0 & 0 & 0 & 0 \\ 0 & 0 & 1 & 0 \\ 0 & 1 & 0 & 0 \\ 0 & 0 & 0 & 0 \end{pmatrix},$$
$$G_3 = \begin{pmatrix} 0 & 0 & 0 & 0 \\ 0 & 0 & 0 & 0 \\ 0 & 0 & 0 & 1 \\ 0 & 0 & 1 & 0 \end{pmatrix}, \tag{11}$$

respectively. Expanding G_1, G_2, and G_3 to Lie algebra, one can get another three elements, such as

$$G_4 = \begin{pmatrix} 0 & 0 & -i & 0 \\ 0 & 0 & 0 & 0 \\ i & 0 & 0 & 0 \\ 0 & 0 & 0 & 0 \end{pmatrix}, \quad G_5 = \begin{pmatrix} 0 & 0 & 0 & 0 \\ 0 & 0 & 0 & -i \\ 0 & 0 & 0 & 0 \\ 0 & i & 0 & 0 \end{pmatrix},$$
$$G_6 = \begin{pmatrix} 0 & 0 & 0 & 1 \\ 0 & 0 & 0 & 0 \\ 0 & 0 & 0 & 0 \\ 1 & 0 & 0 & 0 \end{pmatrix}. \tag{12}$$

Besides, the LR invariant of the four-level system can be described as [40]

$$I(t) = \sum_{m=1}^{6} \eta_m(t) G_m. \tag{13}$$

Combining Eq. (13) with Eqs. (5, 10, 11, 12), one can derive

$$\begin{aligned}
\dot{\eta}_1(t) &= \eta_4(t)\Omega_2(t),\\
\dot{\eta}_2(t) &= -\eta_4(t)\Omega_1(t) + \eta_5(t)\Omega_3(t),\\
\dot{\eta}_3(t) &= -\eta_5(t)\Omega_2(t),\\
\dot{\eta}_4(t) &= \eta_2(t)\Omega_1(t) - \eta_1(t)\Omega_2(t) - \eta_6(t)\Omega_3(t),\\
\dot{\eta}_5(t) &= \eta_6(t)\Omega_1(t) + \eta_3(t)\Omega_2(t) - \eta_2(t)\Omega_3(t),\\
\dot{\eta}_6(t) &= -\eta_5(t)\Omega_1(t) + \eta_4(t)\Omega_3(t).
\end{aligned} \tag{14}$$

By using Eq. (14), the expressions of $\Omega_1(t)$, $\Omega_2(t)$, and $\Omega_3(t)$ can be inversely solved as

$$\begin{aligned}
\Omega_1(t) &= \frac{\eta_5(t)\dot{\eta}_6(t) - \eta_4(t)\dot{\eta}_2(t)}{\eta_4(t)^2 - \eta_5(t)^2},\\
\Omega_2(t) &= \frac{\dot{\eta}_1(t)}{\eta_4(t)},\\
\Omega_3(t) &= \frac{\eta_4(t)\dot{\eta}_6(t) - \eta_5(t)\dot{\eta}_2(t)}{\eta_4(t)^2 - \eta_5(t)^2},
\end{aligned} \tag{15}$$

respectively. Moreover, the constraint relations can also be obtained from Eq. (14) as

$$\sum_{m=1}^{6} \eta_m(t)^2 = \text{Const}, \quad \dot{\eta}_1(t)\eta_5(t) + \dot{\eta}_3(t)\eta_4(t) = 0,$$
$$\eta_4(t)\eta_5(t) + \eta_2(t)\eta_6(t) - \eta_1(t)\eta_3(t) = \text{Const}. \tag{16}$$

$$I(t) = \begin{pmatrix} 0 & \cos\theta & -i\sin\theta\cos\varphi & \cos\theta\sin\varphi \\ \cos\theta & 0 & \sin\theta\sin\varphi & -i\cos\theta\cos\varphi \\ i\sin\theta\cos\varphi & \sin\theta\sin\varphi & 0 & \sin\theta \\ \cos\theta\sin\varphi & i\cos\theta\cos\varphi & \sin\theta & 0 \end{pmatrix}.$$

Thereupon, the orthogonal eigenvectors of $I(t)$ are

$$\begin{aligned}
|\Phi_1(t)\rangle &= \frac{1}{2}\begin{pmatrix} i\cos\varphi - \sqrt{2}\sin\theta\sin\varphi \\ -\sin\varphi + i\sqrt{2}\sin\theta\cos\varphi \\ \sqrt{2}\cos\theta \\ 1 \end{pmatrix},\\
|\Phi_2(t)\rangle &= \frac{1}{2}\begin{pmatrix} i\cos\varphi + \sqrt{2}\sin\theta\sin\varphi \\ -\sin\varphi - i\sqrt{2}\sin\theta\cos\varphi \\ -\sqrt{2}\cos\theta \\ 1 \end{pmatrix},\\
|\Phi_3(t)\rangle &= \frac{1}{2}\begin{pmatrix} -i\cos\varphi + \sqrt{2}\cos\theta\sin\varphi \\ \sin\varphi - i\sqrt{2}\cos\theta\cos\varphi \\ \sqrt{2}\sin\theta \\ 1 \end{pmatrix},\\
|\Phi_4(t)\rangle &= \frac{1}{2}\begin{pmatrix} -i\cos\varphi - \sqrt{2}\cos\theta\sin\varphi \\ \sin\varphi + i\sqrt{2}\cos\theta\cos\varphi \\ -\sqrt{2}\sin\theta \\ 1 \end{pmatrix},
\end{aligned} \tag{20}$$

Considering the constraint relations in Eq. (16), we assume

$$\begin{aligned}
\eta_1(t) &= \cos\theta, \quad \eta_2(t) = \sin\theta\sin\varphi,\\
\eta_3(t) &= \sin\theta, \quad \eta_4(t) = \sin\theta\cos\varphi,\\
\eta_5(t) &= \cos\theta\cos\varphi, \quad \eta_6(t) = \cos\theta\sin\varphi,
\end{aligned} \tag{17}$$

in which θ and φ are time-dependent parameters. By substituting Eq. (17) into Eq. (15), the detailed expressions of the Rabi frequencies can be derived as

$$\begin{aligned}
\Omega_1(t) &= \dot{\theta}\tan 2\theta\tan\varphi - \dot{\varphi},\\
\Omega_2(t) &= -\dot{\theta}/\cos\varphi,\\
\Omega_3(t) &= \dot{\theta}\tan\varphi/\cos 2\theta.
\end{aligned} \tag{18}$$

Up to now, by means of designing the Rabi frequencies $\Omega_1(t)$, $\Omega_2(t)$, and $\Omega_3(t)$, we can reversely construct the Hamiltonian $H_{\text{eff}}(t)$ in Eq. (9) to drive a particular initial state to a specific final state. Before designing the Rabi frequencies, it is necessary to know the boundary conditions of the time-dependent parameters $\theta(t)$ and $\varphi(t)$. The boundary conditions are decided by the initial state and the final state, which can be expressed as $|\Psi(0)\rangle$ and $|\Psi(T)\rangle$, respectively, where T represents the final time. As shown in Eq. (6), the state of the total four-level system $|\Psi(t)\rangle$ contains a LR phase $\alpha_n(t)$ $(n = 1, 2, 3, 4)$. Therefore, it is indispensable to obtain the phase. Based on Eq. (17), the LR invariant in Eq. (13) can be rewritten as

with corresponding eigenvalues 0, 0, $\sqrt{2}$, and $-\sqrt{2}$, respectively. With the help of Eqs. (7, 9, 18, 20), the derivatives of the LR phases with respect to time are given by

$$\begin{aligned}
\dot{\alpha}_1(t) &= -\sqrt{2}\dot{\theta}\cos\theta\tan\varphi/\cos 2\theta = -\sqrt{2}\Omega_3(t)\cos\theta,\\
\dot{\alpha}_2(t) &= \sqrt{2}\dot{\theta}\cos\theta\tan\varphi/\cos 2\theta = \sqrt{2}\Omega_3(t)\cos\theta,\\
\dot{\alpha}_3(t) &= -\sqrt{2}\dot{\theta}\sin\theta\tan\varphi/\cos 2\theta = -\sqrt{2}\Omega_3(t)\sin\theta,\\
\dot{\alpha}_4(t) &= \sqrt{2}\dot{\theta}\sin\theta\tan\varphi/\cos 2\theta = \sqrt{2}\Omega_3(t)\sin\theta,
\end{aligned} \tag{21}$$

according to the orthogonal eigenvectors $|\Phi_1(t)\rangle$, $|\Phi_2(t)\rangle$, $|\Phi_3(t)\rangle$, and $|\Phi_4(t)\rangle$, respectively.

Now we can use the LR theory to transfer a particular initial state into a specific final state. Here, the initial and final state are assumed as $|\Psi(0)\rangle = |W_r\rangle$ and $|\Psi(T)\rangle = |\text{GHZ}_r\rangle$, respectively. For simplicity, we set $\varphi(0) = \theta(0) = 0$ and expand the final state $|\Psi(T)\rangle$ by Eqs. (6, 8, 20, 21) as

$$|\Psi(T)\rangle = \frac{i}{\sqrt{2}} e^{i\alpha_3(T)}|\Phi_3(T)\rangle - \frac{i}{\sqrt{2}} e^{i\alpha_4(T)}|\Phi_4(T)\rangle. \tag{22}$$

To achieve the transition $\mathcal{T}_1$, $|\Psi(0)\rangle = |W_r\rangle \rightarrow |\mathrm{GHZ}_r\rangle = |\Psi(T)\rangle$, boundary conditions $\alpha_3(T) = -\pi/2$, $\alpha_4(T) = \pi/2$, and $\varphi(T) = 0$ should be set.

On the contrary, if the initial state is $|\Psi(0)\rangle = |\mathrm{GHZ}_r\rangle$ and the final state is $|\Psi(T)\rangle = |W_r\rangle$, the boundary condition $\varphi(0) = \theta(0) = 0$ is chosen for the brief and the final state can be expanded as

$$|\Psi(T)\rangle = \frac{1}{\sqrt{2}} e^{i\alpha_3(T)} |\Phi_3(T)\rangle + \frac{1}{\sqrt{2}} e^{i\alpha_4(T)} |\Phi_4(T)\rangle. \quad (23)$$

By setting $\alpha_3(T) = \pi/2$, $\alpha_4(T) = -\pi/2$, $\varphi(T) = 0$, and $\theta(T) = 0$, one can realize the transition $\mathcal{T}_2$: $|\Psi(0)\rangle = |\mathrm{GHZ}_r\rangle \rightarrow |W_r\rangle = |\Psi(T)\rangle$.

In summary, the boundary conditions are

$$\varphi(0) = \varphi(T) = \theta(0) = 0, \quad \alpha_4(T) = -\alpha_3(T) = \pi/2, \quad (24)$$

in the transition $\mathcal{T}_1$ and

$$\varphi(0) = \varphi(T) = \theta(0) = \theta(T) = 0,$$
$$\alpha_3(T) = -\alpha_4(T) = \pi/2, \quad (25)$$

in the transition $\mathcal{T}_2$. According to the boundary conditions in Eqs. (24, 25), the time-dependent parameters $\varphi(t)$ and $\theta(t)$ are given by

$$\varphi(t) = a \sin(\pi t/T) \sin(2\pi t/T),$$
$$\theta(t) = b \sin^2(\pi t/T), \quad (26)$$

where a and b are parameters controlling the maximal value of $\varphi(t)$ and $\theta(t)$, respectively. Note that $\varphi(t)$ and $\theta(t)$ should meet the equation $\alpha_3(T) = \sqrt{2}\int_0^T \Omega_3(t) \sin[\theta(t)]dt = -\pi/2$ in transition $\mathcal{T}_1$ and the equation $\alpha_3(T) = \sqrt{2}\int_0^T \Omega_3(t) \sin[\theta(t)]dt = \pi/2$ in transition $\mathcal{T}_2$. These two equations restrict the relations between parameters a and b. For ease of reading, we list the relations between a and b of transitions $\mathcal{T}_1$ and $\mathcal{T}_2$ in Tables I and II, respectively.

Based on the results in Tables I and II, $a = 0.42\pi$ and $b = 0.7069$ are chosen for transition $\mathcal{T}_1$, and $a = 0.42\pi$ and $b = -0.7069$ are chosen for transition $\mathcal{T}_2$. Thus, by exploiting Eqs. (18, 26), we can obtain the Rabi frequencies of the effective Hamiltonian $H_{\mathrm{eff}}(t)$ to realize the transitions $\mathcal{T}_1$ and $\mathcal{T}_2$. The Rabi frequencies of pulses in transitions $\mathcal{T}_1$ and $\mathcal{T}_2$ are plotted in Figs. 3(a) and 3(b), respectively. Moreover, the fidelities of transitions $\mathcal{T}_1$ and $\mathcal{T}_2$ are plotted in Figs. 3(c) and 3(d), respectively. From Figs. 3(a) and 3(b), one can see that all the Rabi frequencies of pulses vanish at the initial time and the final time, which means the pulses will be easy to open and shut off. In Figs. 3(c) and 3(d), the fidelities

TABLE I. a and corresponding b in transition $\mathcal{T}_1$.

a	b
$0.42\,\pi$	0.7069
$0.40\,\pi$	0.7226
$0.38\,\pi$	0.7304
$0.36\,\pi$	0.7450
$0.35\,\pi$	0.7461
$0.34\,\pi$	0.7540
$0.32\,\pi$	0.7618
$0.30\,\pi$	0.7697

TABLE II. a and corresponding b in transition $\mathcal{T}_2$.

a	b
$0.42\,\pi$	–0.7069
$0.40\,\pi$	–0.7226
$0.38\,\pi$	–0.7304
$0.36\,\pi$	–0.7450
$0.35\,\pi$	–0.7461
$0.34\,\pi$	–0.7540
$0.32\,\pi$	–0.7618
$0.30\,\pi$	–0.7697

for the transitions $\mathcal{T}_1$ and $\mathcal{T}_2$ both reach 100%. In a word, based on the LR invariant and Lie algebra in a four-level system, we inversely build the effective Hamiltonian $H_{\mathrm{eff}}(t)$ to implement transition $\mathcal{T}_1$: $|\Psi(0)\rangle = |W_r\rangle \rightarrow |\mathrm{GHZ}_r\rangle = |\Psi(T)\rangle$ and transition $\mathcal{T}_2$: $|\Psi(0)\rangle = |\mathrm{GHZ}_r\rangle \rightarrow |W_r\rangle = |\Psi(T)\rangle$. Since one can convert a W state into a GHZ state by choosing

$$\Omega_{r1}(t) = -i\Omega_1(t)/\sqrt{3}, \quad \Omega_{r2}(t) = \Omega_2(t)/2,$$
$$\Omega_{r3}(t) = \Omega_3(t)/\sqrt{3}, \quad a = 0.42\pi, \quad b = 0.7069, \quad (27)$$

with the expressions of $\Omega_1(t)$, $\Omega_2(t)$, and $\Omega_3(t)$ shown in Eqs. (18, 26).

Analogously, one can also choose

$$\Omega_{r1}(t) = -i\Omega_1(t)/\sqrt{3}, \quad \Omega_{r2}(t) = \Omega_2(t)/2,$$
$$\Omega_{r3}(t) = \Omega_3(t)/\sqrt{3}, \quad a = 0.42\pi, \quad b = -0.7069 \quad (28)$$

to convert a GHZ state to a W state.

IV. NUMERICAL SIMULATIONS

In this section, first of all, considering the decoherence caused by the thermal noise, the dephasing, and the spontaneous emission, we give numerical simulations of fidelities for the interconversions between the GHZ states and the W states based on the master equation [42]:

$$\dot{\rho}(t) = i[\rho(t), H(t)] + D_{\mathrm{deph}}[\rho(t)] + D_{\mathrm{therm}}[\rho(t)],$$
$$D_{\mathrm{deph}}[\rho(t)] = \sum_{l=4}^{6} \left[L_l \rho L_l^\dagger - \frac{1}{2}(L_l^\dagger L_l \rho + \rho L_l^\dagger L_l) \right],$$
$$D_{\mathrm{therm}}[\rho(t)] = \sum_{l=1}^{3} \left\{ (\bar{n}+1) \left[L_l \rho L_l^\dagger - \frac{1}{2}(L_l^\dagger L_l \rho + \rho L_l^\dagger L_l) \right] \right.$$
$$\left. + \bar{n} \left[L_l^\dagger \rho L_l - \frac{1}{2}(L_l L_l^\dagger \rho + \rho L_l L_l^\dagger) \right] \right\}, \quad (29)$$

where $H(t)$ is the original Hamiltonian shown in Eq. (1), $\rho(t)$ is the density matrix of the total system, and $\bar{n}$ is the average number of thermal phonons. Besides, L_l ($l = 1, 2, \ldots, 6$) are the Lindblad operators as

$$L_1 = \sqrt{\Gamma_1}|0\rangle_1\langle r|, \quad L_2 = \sqrt{\Gamma_2}|0\rangle_2\langle r|,$$
$$L_3 = \sqrt{\Gamma_3}|0\rangle_3\langle r|, \quad L_4 = \sqrt{\gamma_1}(|r\rangle_1\langle r| - |0\rangle_1\langle 0|),$$
$$L_5 = \sqrt{\gamma_2}(|r\rangle_2\langle r| - |0\rangle_2\langle 0|),$$
$$L_6 = \sqrt{\gamma_3}(|r\rangle_3\langle r| - |0\rangle_3\langle 0|), \quad (30)$$

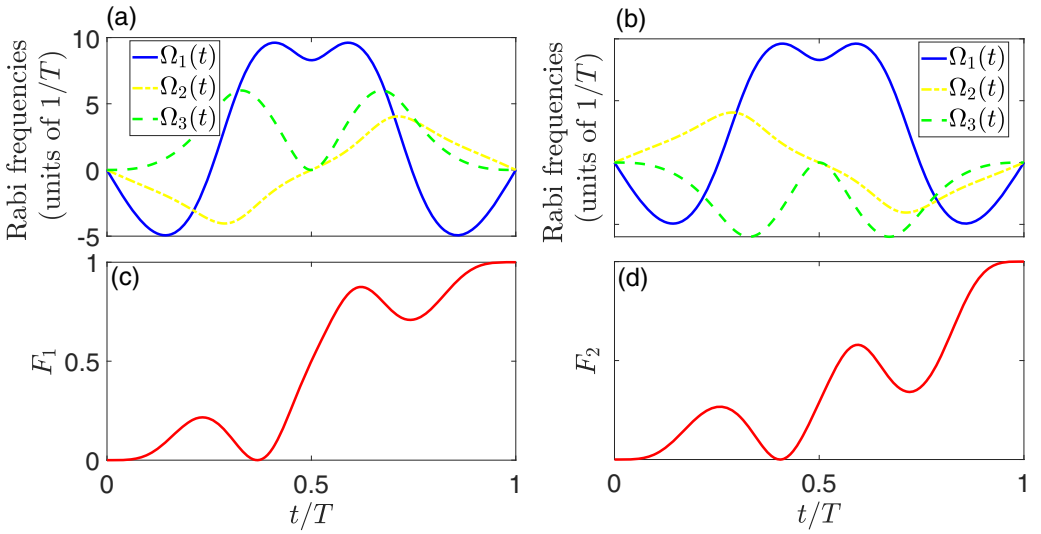

FIG. 3. (a) Rabi frequencies $\Omega_1(t)$, $\Omega_2(t)$, and $\Omega_3(t)$ vs t/T in the transition $\mathcal{T}_1$. (b) Rabi frequencies $\Omega_1(t)$, $\Omega_2(t)$, and $\Omega_3(t)$ vs t/T in the transition $\mathcal{T}_2$. (c) Fidelity F_1 vs t/T in $\mathcal{T}_1$. (d) Fidelity F_2 vs t/T in $\mathcal{T}_2$.

with Γ_k $(k = 1, 2, 3)$ being the spontaneous emission rate of the path $|r\rangle_k \to |0\rangle_k$ and γ_k being the dephasing rate of the kth atom. Here $\gamma_1 = \gamma_2 = \gamma_3 = \gamma$ and $\Gamma_1 = \Gamma_2 = \Gamma_3 = \Gamma$ are set for simplicity.

Based on the experimental parameters realized in protocol [43], a group of parameters, $V = 2\pi \times$ 50 MHz and $\Omega_{r4} = 23.56$ MHz, is chosen. In this case, the total evolution time is $T = 17.83$ μs here, which is short enough compared with the lifetime and operation time of the neutral atoms [44]. Combining the value of T with Fig. 3(a), Fig. 3(b), and Eqs. (27, 28), the maximal values of Rabi frequencies can be derived as $\max[\Omega_{r1}(t)] = 0.31$ MHz, $\max[\Omega_{r2}(t)] = 0.11$ MHz, and $\max[\Omega_{r3}(t)] = 0.19$ MHz. In addition, we set $\Delta_4 = 2\pi \times$ 150 MHz, which is experimentally acceptable [43,45]. Moreover, ranges for the spontaneous emission Γ as $0 \sim 2$ kHz [44] and the dephasing rate γ as $0 \sim 1$ kHz are chosen here. The average number of thermal phonons $\bar{n}$ is set in a scope as $0 \sim 1$. Considering the Bose-Einstein distribution, the average number of thermal phonons is given by $\bar{n} = 1/(e^{\frac{\hbar\omega}{k_B T}} - 1)$. Assuming the frequency of thermal noise as $\omega = 2\pi \times 1$ MHz, the scope of $\bar{n}$ can be understood as the range of experimental temperature, $0 \sim 68.31$ μK.

By substituting the parameters into the master equation in Eqs. (29, 30), the density matrix $\rho(t)$ could be numerically solved. Then we can obtain the fidelity for converting a W state to a GHZ state by utilizing $F_1 = |\langle \mathrm{GHZ}_r|\rho_1(T)|\mathrm{GHZ}_r\rangle|$ and the fidelity for transforming a GHZ state into a W state with $F_2 = |\langle W_r|\rho_2(T)|W_r\rangle|$. Note that $\rho_1(t)$ corresponds to the initial state $|W_r\rangle$ and $\rho_2(t)$ corresponds to the initial state $|\mathrm{GHZ}_r\rangle$ here. We show the relations of F_1 (F_2) versus the spontaneous emission rate Γ and the dephasing rate γ in Fig. 4(a) [Fig. 4(b)] with $\bar{n} = 0$. From Figs. 4(a) and 4(b), one could find the fidelities F_1 and F_2 are both robust against the spontaneous emission rate Γ and the dephasing rate γ. Besides, the relations of F_1 (F_2) versus the spontaneous emission rate Γ and the average number of thermal phonons $\bar{n}$ are demonstrated in Fig. 5(a) [Fig. 5(b)] with setting $\gamma = 0$. Figures 5(a) and 5(b) prove that the protocol cannot be easily influenced by the spontaneous emission and the thermal noise. By considering a group of parameters such as $\Gamma = 1.2$ kHz, $\gamma = 1$ kHz, and $\bar{n} = 0.2$ (i.e., experimental temperature being 26.81 μK [46]), one can obtain $F_1 = 91.12\%$ and $F_2 = 91.18\%$, which are receivable values in experiments.

Second, taking the parametric errors in experiments into account, we discuss the influence of fidelities for the interconversions by introducing the systematic error on Rabi frequencies $\Omega_{rk}(t)$ $(k = 1, 2, 3)$. Here, after considering systematic errors, the real Rabi frequency can be written as

$$\Omega'_{rk}(t) = (1 + \eta)\Omega_{rk}(t), \tag{31}$$

where η is the coefficient of the systematic error on Rabi frequency $\Omega_{rk}(t)$. By substituting the real Rabi frequency $\Omega'_{rk}(t)$ into Eqs. (29, 30) and setting $\bar{n} = \Gamma = \gamma = 0$, we can numerically calculate $\rho(t)$ and afterwards derive the final fidelities F_1 and F_2. The relations between final fidelity F_1 (F_2) and η are plotted in Fig. 6. One can see from Fig. 6 that even if the coefficient of the systematic errors reaches $\pm 10\%$, the fidelities F_1 and F_2 are higher than 97%. Thus, the influence of the systematic errors on Rabi frequencies is weak in the present protocol.

In addition, it is appropriate to consider the frequency mismatching. Under actual experimental conditions, the

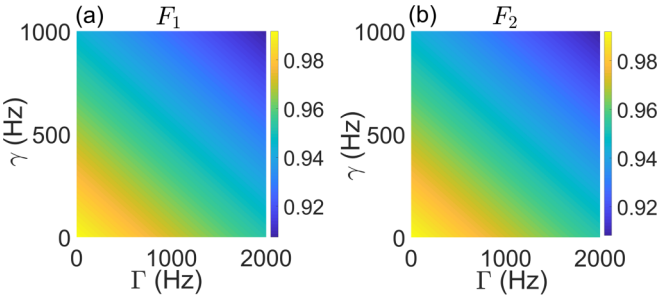

FIG. 4. (a) Fidelity F_1 vs the spontaneous emission rate Γ and the dephasing rate γ. (b) The fidelity F_2 vs the spontaneous emission rate Γ and the dephasing rate γ.

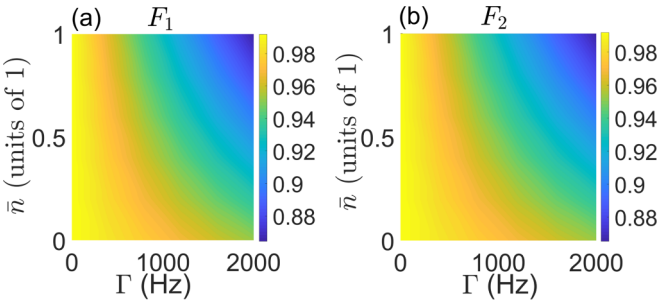

FIG. 5. (a) Fidelity F_1 vs the spontaneous emission rate Γ and the average number of thermal phonons $\bar{n}$. (b) Fidelity F_2 vs the spontaneous emission rate Γ and the average number of thermal phonons $\bar{n}$.

frequency matching may not be completely satisfied. Therefore, the real values of detuning of Rabi frequency $\Omega_{rk}(t)$ are assumed as

$$\begin{aligned}\delta_1' &= (1+\mu)\delta_1,\\ \delta_2' + \Delta_2 &= (1+\mu)\delta_2 + \Delta_2,\\ \delta_3' + \Delta_3 &= (1+\mu)\delta_3 + \Delta_3,\end{aligned} \tag{32}$$

with μ being the error rate and δ_1, $\delta_2' + \Delta_2$ and $\delta_3' + \Delta_3$ being the ideal values of the detuning of Rabi frequency $\Omega_{rk}(t)$, respectively. Through the same calculative process, the relationships between final fidelities F_1 and F_2 and error rate μ are plotted in Fig. 7, respectively. Note that $\bar{n} = \Gamma = \gamma = \eta = 0$ is set here. From Fig. 7, one can find that the fidelities F_1 and F_2 are both higher than 95% when the error rate of frequency matching is $\mu = 1\%$. Therefore, the protocol is also robust against frequency mismatching.

V. EXPANSION

With multiparticle entanglement (the number of particles $N \geqslant 4$) being popular in recent research [47,48], it is meaningful to implement the interconversions between the N-qubit GHZ states and the N-qubit W states, whose definitions are

$$\begin{aligned}|\mathrm{GHZ}_r\rangle &= (|0\rangle^{\otimes N} + |r\rangle^{\otimes N})/\sqrt{2},\\ |W_r\rangle &= \frac{1}{\sqrt{N}}\sum_{n=1}^{N}\sigma_n^+|0\rangle^{\otimes N},\end{aligned} \tag{33}$$

respectively, in which $\sigma_n^+ = |r\rangle_n\langle 0|$ is the raising operator of the nth atom. Similarly, we can also construct a system

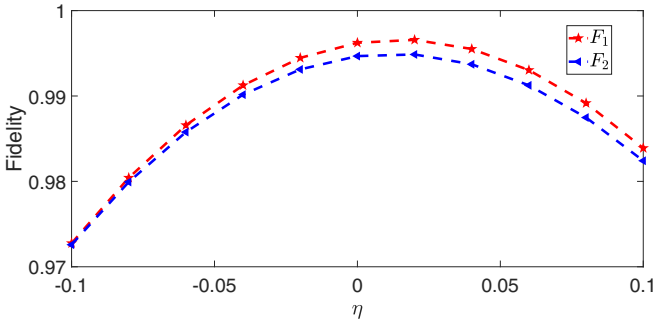

FIG. 6. Fidelities F_1 and F_2 vs the systematic errors rate η with red astroid line and blue triangular line, respectively.

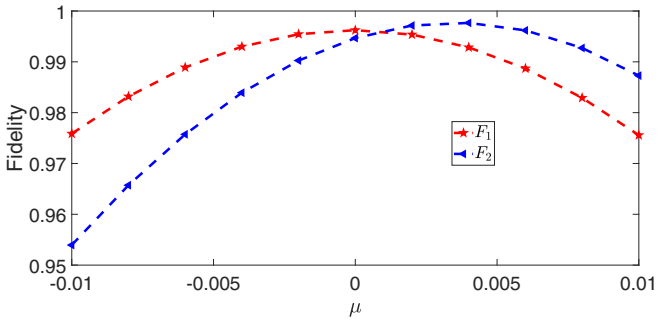

FIG. 7. Fidelities F_1 and F_2 vs the error rate of frequency matching μ with red astroid line and blue triangular line, respectively.

by N neutral atoms with Rydberg states and refine the total Hamiltonian into

$$H_{\mathrm{eff}}(t) = \sum_{m=1}^{N}\Omega_m(t)|(m-1)r\rangle\langle mr|, \tag{34}$$

where $|mr\rangle$ denotes the collection of the total state including m Rydberg states, which can be indicated as

$$|mr\rangle = \sum_{q_1<q_2<\cdots<q_m} a_{q_1,q_2,\ldots,q_m} \times \sigma_{q_1}^+\sigma_{q_2}^+\ldots\sigma_{q_m}^+|0\rangle^{\otimes N}, \tag{35}$$

with $\sigma_{q_1}^+ = |r\rangle_{q_1}\langle 0|$, $\sigma_{q_2}^+ = |r\rangle_{q_2}\langle 0|$,..., $\sigma_{q_m}^+ = |r\rangle_{q_m}\langle 0|$ being the raising operators of atoms q_1, q_2,..., q_m ($\{q_1, q_2,\ldots, q_m\} \in \{1, 2,\ldots, N\}$, $q_1 < q_2 < \cdots < q_m$), respectively, and $a_{p,q,\ldots,l}$ is the coefficient of state $\sigma_{q_1}^+\sigma_{q_2}^+\cdots\sigma_{q_m}^+|0\rangle^{\otimes N}$. Note that when $m = 1$ is satisfied, the coefficient a_{q_1} is always equal to $1/\sqrt{N}$, i.e., $|1r\rangle$ is another expression of the N-qubit W states $|W_r\rangle$.

It is clear that $H_{\mathrm{eff}}(t)$ is $(N+1)$ level. In order to realize the interconversions between the N-qubit GHZ states $(|0r\rangle + |Nr\rangle)/\sqrt{2}$ and the N-qubit W states $|1r\rangle$, an invariant $I(t)$ for an $(N+1)$-level system should be structured. By utilizing $i\frac{\partial I(t)}{\partial t} - [H_{\mathrm{eff}}(t), I(t)] = 0$, one can get a set of equations which will provide an expression of the Rabi frequency $\Omega_m(t)$. Using these expressions and suitable boundary conditions, we can reversely construct the Rabi frequency $\Omega_m(t)$ for the interconversions between the N-qubit GHZ states and the N-qubit W states.

For example, to realize the interconversions in a 4-qubit system, an analogical atomic model shown in Fig. 2 is used with expansion to four Rydberg atoms. The transition $|0\rangle_k \leftrightarrow |r\rangle_k$ (now $k = 1, 2, 3, 4$), is driven by four time-dependent Rabi frequencies $\Omega_{r1}(t)$, $\Omega_{r2}(t)$, $\Omega_{r3}(t)$, $\Omega_{r4}(t)$ and one time-independent Rabi frequency Ω_{r5}, whose detunings are δ_1, $\Delta_2 + \delta_2$, $\Delta_3 + \delta_3$, $\Delta_4 + \delta_4$, and Δ_5, respectively. Also, each two adjacent atoms own Rydberg interaction strength V. In the interaction picture, the Hamiltonian yields ($p, q, k = 1, 2, 3, 4$)

$$\begin{aligned}H(t) = \sum_{k=1}^{4}[&\Omega_{r1}(t)e^{-i\delta_1 t} + \Omega_{r2}(t)e^{-i(\delta_2+\Delta_2)t}\\ &+ \Omega_{r3}(t)e^{-i(\delta_3+\Delta_3)t} + \Omega_{r4}(t)e^{-i(\delta_4+\Delta_4)t}\\ &+ \Omega_{r5}e^{i\Delta_5 t}]|r\rangle_k\langle 0| + \mathrm{H.c.} + \sum_{p<q}V|rr\rangle_{pq}\langle rr|,\end{aligned} \tag{36}$$

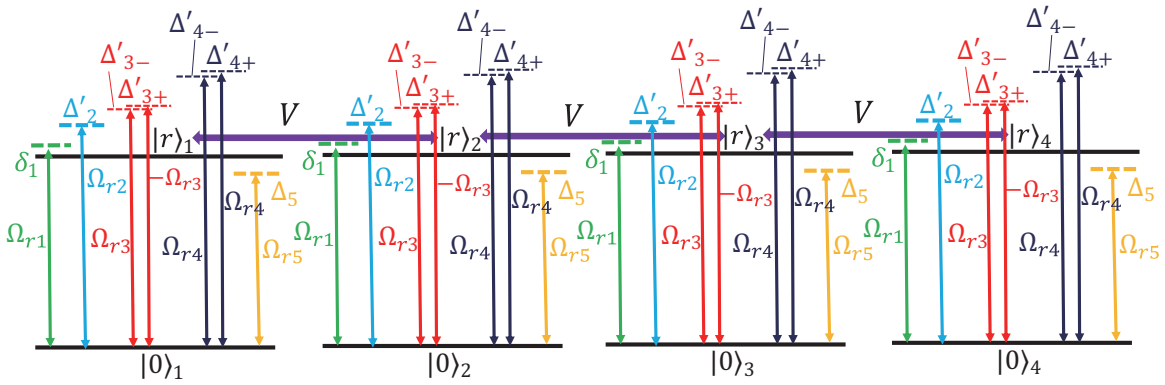

FIG. 8. The physical model for realizing the interconversions between the GHZ states and the W states in a 4-qubit system, with $\Delta'_2 = \Delta_2 + \delta_2$, $\Delta'_{3+} = \Delta_3 + \delta_3 + \xi$, $\Delta'_{3-} = \Delta_3 + \delta_3 - \xi$, $\Delta'_{4+} = \Delta_4 + \delta_4 + \xi$, and $\Delta'_{4-} = \Delta_4 + \delta_4 - \xi$.

with conditions $\Delta_2 = V$, $\Delta_3 = 2V$, $\Delta_4 = 3V$, and $\{V,\ \Delta_5\} \gg \{\Omega_{r5},\ \delta_k\} \gg \max\{|\Omega_{rk}(t)|\}$. The detailed processes for deriving the effective Hamiltonian is analogously shown in Appendix (3-qubit system). By choosing

$$\begin{aligned}
\delta_1 &= \frac{8\Omega_5^2}{\Delta_5} - \frac{6\Omega_5^2}{\Delta_5 + V},\\
\delta_2 &= -\frac{4\Omega_5^2}{\Delta_5} + \frac{12\Omega_5^2}{\Delta_5 + V} - \frac{6\Omega_5^2}{\Delta_5 + 2V},\\
\delta_3 &= -\frac{6\Omega_5^2}{\Delta_5 + V} + \frac{12\Omega_5^2}{\Delta_5 + 2V} - \frac{4\Omega_5^2}{\Delta_5 + 3V},\\
\delta_4 &= -\frac{6\Omega_5^2}{\Delta_5 + 2V} + \frac{8\Omega_5^2}{\Delta_5 + 3V},
\end{aligned} \tag{37}$$

the effective Hamiltonian is given by

$$\begin{aligned}
H_{\rm eff}^{(4)}(t) = {} & 2\Omega_{r1}(t)|0r\rangle\langle 1r| + \sqrt{6}\Omega_{r2}(t)|1r\rangle\langle 2r|\\
& + \sqrt{6}\Omega_{r3}(t)|2r\rangle\langle 3r| + 2\Omega_{r4}(t)|3r\rangle\langle 4r| + \text{H.c.},
\end{aligned} \tag{38}$$

with $|0r\rangle = |0000\rangle$, $|1r\rangle = (|000r\rangle + |00r0\rangle + |0r00\rangle + |r000\rangle)/2$, $|2r\rangle = (|r00r\rangle + |r0r0\rangle + |rr00\rangle + |0rr0\rangle + |0r0r\rangle + |00rr\rangle)/\sqrt{6}$ and $|4r\rangle = |rrrr\rangle$. It is clear that $|1r\rangle$ is a 4-qubit W state, and a 4-qubit GHZ state reads $[(|0r\rangle + |4r\rangle)/\sqrt{2}]$. For realizing interconversions between them, a five-level invariant $I(t)$ should be construct. However, such an invariant is hard to find. We therefore change the effective Hamiltonian $H_{\rm eff}^{(4)}(t)$ in Eq. (38) to

$$\begin{aligned}
H_{\rm eff}^{(4)'}(t) = {} & 2\Omega_{r1}(t)|0r\rangle\langle 1r| + \sqrt{6}\Omega_{r2}(t)|1r\rangle\langle 2r|\\
& + [\sqrt{6}\Omega_{r3}(t)(e^{i\xi t} - e^{-i\xi t})]|2r\rangle\langle 3r|\\
& + [2\Omega_{r4}(t)(e^{i\xi t} + e^{-i\xi t})]|3r\rangle\langle 4r| + \text{H.c.},
\end{aligned} \tag{39}$$

with additional detuning $\xi \gg \max\{|\Omega_{rk}(t)|\}$. Observe that the original Hamiltonian corresponding to such $H_{\rm eff}^{(4)'}(t)$ can be achieved via adjusting the detuning of $\Omega_{r3}(t)$ as $\Delta_3 + \delta_3 - \xi$ and the detuning of $\Omega_{r4}(t)$ as $\Delta_4 + \delta_4 - \xi$, besides adding two extra Rabi frequencies $-\Omega_{r3}(t)$ and $\Omega_{r4}(t)$ with detunings $\Delta_3 + \delta_3 + \xi$ and $\Delta_4 + \delta_4 + \xi$, respectively.

For the sake of easy understanding, a figure for detailing the physical model corresponding to the modified original Hamiltonian is shown in Fig. 8. The modified effective Hamiltonian $H_{\rm eff}^{(4)'}(t)$ in Eq. (39) can be further calculated by second-order perturbation theory and refined like

$$\begin{aligned}
H_{\rm eff}^{(4)''}(t) = {} & 2\Omega_{r1}(t)|0r\rangle\langle 1r| + \sqrt{6}\Omega_{r2}(t)|1r\rangle\langle 2r|\\
& + \left[\frac{4\sqrt{6}\Omega_{r3}(t)\Omega_{r4}(t)}{\xi}\right]|2r\rangle\langle 4r| + \text{H.c.},
\end{aligned} \tag{40}$$

which is now a four-level effective Hamiltonian [$\Omega_{rk}(t)$ being real]. Therefore, the results in Sec. III are still valid. Since one can convert a 4-qubit W state into a 4-qubit GHZ state by choosing

$$\begin{aligned}
&\Omega_{r1}(t) = -i\Omega_1(t)/2, \quad \Omega_{r2}(t) = \Omega_2(t)/\sqrt{6},\\
&\Omega_{r3}(t) = \Omega_{r4}(t) = \sqrt{\frac{\xi\Omega_3(t)}{4\sqrt{6}}},\\
&a = 0.42\pi, \quad b = 0.7069,
\end{aligned} \tag{41}$$

as well as choosing

$$\begin{aligned}
&\Omega_{r1}(t) = -i\Omega_1(t)/2, \quad \Omega_{r2}(t) = \Omega_2(t)/\sqrt{6},\\
&\Omega_{r3}(t) = -\Omega_{r4}(t) = \sqrt{-\frac{\xi\Omega_3(t)}{4\sqrt{6}}},\\
&a = 0.42\pi, \quad b = -0.7069,
\end{aligned} \tag{42}$$

to covert a 4-qubit GHZ state to a 4-qubit W state, with the expressions of $\Omega_1(t)$, $\Omega_2(t)$ and $\Omega_3(t)$ shown in Eqs. (18, 26). The fidelities for such interconversions are indicated in Fig. 9. With considering a group of parameters such as $T = 20\,\mu$s, $\Omega_{r5} = 25$ MHz, $V = 175$ MHz, $\xi = 5$ MHz, and $\Delta_5 = 1.25$ GHz [49], the fidelities for both conversions are close to 99%, apparently showing the feasibility of the present protocol in a multiparticle ($N \geqslant 4$) system.

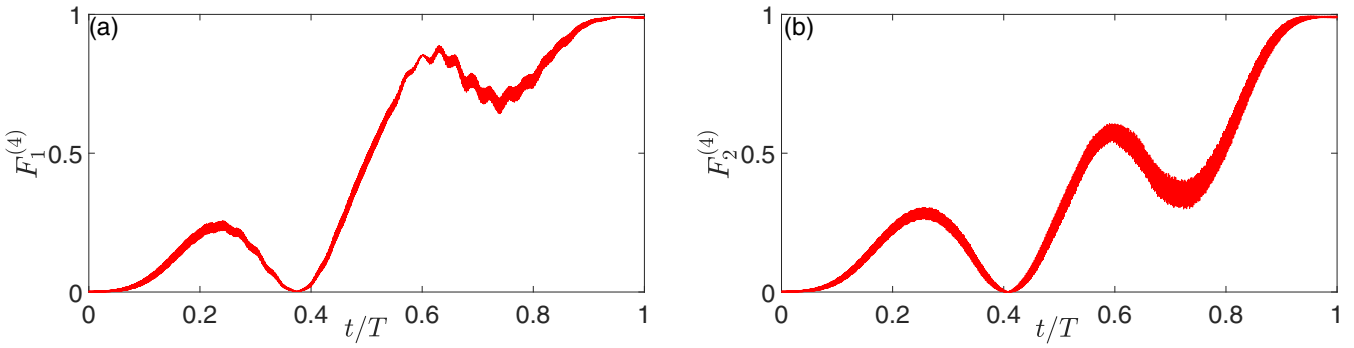

FIG. 9. (a) Fidelity $F_1^{(4)}$ vs t/T for converting the 4-qubit W states into 4-qubit GHZ states. (b) Fidelity $F_2^{(4)}$ (converting the 4-qubit GHZ states into 4-qubit W states) vs t/T. Observe that compared with Figs. 3(c) and 3(d), some oscillations arise in Figs. 9(a) and 9(b). Such a phenomenon is caused by the incomplete satisfaction of condition $\Delta_5 \gg \Omega_5$, however, slightly reducing the final fidelities. By choosing the parameters $T = 20\,\mu$s, $\Omega_{r5} = 25$ MHz, $V = 175$ MHz, $\xi = 5$ MHz, and $\Delta_5 = 1.25$ GHz, we obtain $F_1^{(4)} = 98.91\%$ and $F_2^{(4)} = 99.18\%$. For raising these fidelities, one can increase the value of Δ_5, i.e., more strictly satisfying condition $\Delta_5 \gg \Omega_5$, nevertheless leading to the difficulty of the experiment.

VI. CONCLUSION

In summary, we have presented a protocol for the deterministic interconversions (one step) between GHZ and W states in an atomic system. We use the Rydberg interactions among three neutral atoms with Rydberg states to build nonlocal operations for realizing the interconversions. The effective Hamiltonian of the physical model can be finally simplified as a four-level Hamiltonian with basis $\{|000\rangle, |W_r\rangle, |W_r'\rangle, |rrr\rangle\}$. Next, the Lie algebra is used to structure a LR invariant, and we afterwards exploit the invariant to design appropriate Rabi frequencies of the effective Hamiltonian for the interconversions. In order to check the correctness and feasibility of the protocol, we carry out numerical simulations by taking the thermal noise, dephasing, spontaneous emission, systematic errors, and frequency mismatching into account. By considering a group of experimentally feasible parameters such as $V = 2\pi \times 50$ MHz, $\Omega_{r4} = 23.56$ MHz, $\Delta_4 = 2\pi \times 150$ MHz, $T = 17.83\ \mu$s, $\max[\Omega_{r1}(t)] = 0.31$ MHz, $\max[\Omega_{r2}(t)] = 0.11$ MHz, $\max[\Omega_{r3}(t)] = 0.19$ MHz, $\Gamma = 1.2$ kHz, $\bar{n} = 0.2$, and $\gamma = 1$ kHz, we can obtain the fidelity F_1 of conversion $|W_r\rangle \to |\mathrm{GHZ}_r\rangle$ as $F_1 = 91.12\%$ and the fidelity F_2 of conversion $|\mathrm{GHZ}_r\rangle \to |W_r\rangle$ as $F_2 = 91.18\%$. This means both fidelities F_1 and F_2 are robust against the decoherence. Besides, the influence of the systematic error on Rabi frequency $\Omega_{rk}(t)$ and the frequency mismatching is also discussed. When the coefficient of the systematic errors η reaches 10%, the fidelities F_1 and F_2 are still higher than 97%. When the error rate μ of frequency matching is 1%, the fidelities F_1 and F_2 are higher than 95%. In a word, the protocol is stable against spontaneous emission of the Rydberg state $|r\rangle_k$, the thermal noise, the dephasing, the systematic errors on Rabi frequency $\Omega_{rk}(t)$, and the frequency mismatching, that is, the protocol is experimentally feasible. Moreover, we briefly expand the protocol to a multiparticle ($N \geqslant 4$) system and give detailed processes for the interconversions between the 4-qubit GHZ states and the 4-qubit W states with high fidelities.

Compared with two representative works [34,35] about converting the W states into the GHZ states based on an atomic system, our protocol has the following advantages:

(i) Protocol [35] is probabilistic with maximally 75% success probability. In the present protocol, the success probabilities are 100%.

(ii) The conversions in both protocols [34,35] are irreversible from the W states to the GHZ states, which may be limited when one needs to convert the GHZ states into the W states. In the present protocol, the conversions are two-way and both ways have high fidelities. Ergo, the protocol might be more flexible in some situations.

Therefore, the present protocol may be helpful for conversions between entanglements and can further improve the efficiency of some quantum information tasks. We hope the protocol can soon be realized experimentally.

ACKNOWLEDGMENT

This work was supported by the National Natural Science Foundation of China under Grants No. 11575045, No. 11374054, No. 11674060, and No. 11805036.

APPENDIX: DETAILED PROOF FROM EQ. (1) TO EQ. (2)

By using second-order perturbation theory, the effective Hamiltonian $H_{e1}(t)$ can be preliminarily calculated as

$$
\begin{aligned}
H_{e1}(t) &= H_{e10} + H_{e1i}(t),\\
H_{e10} &= -3\frac{\Omega_{r4}^2}{\Delta_4}|000\rangle\langle 000| + \frac{3\Omega_{r4}^2}{\Delta_4 + 2V}|rrr\rangle\langle rrr|\\
&\quad + 3\left(\frac{\Omega_{r4}^2}{\Delta_4 + V} - \frac{\Omega_{r4}^2}{\Delta_4 + 2V}\right)|W_r'\rangle\langle W_r'|\\
&\quad + 3\left(\frac{\Omega_{r4}^2}{\Delta_4} - \frac{\Omega_{r4}^2}{\Delta_4 + V}\right)|W_r\rangle\langle W_r|\\
&\quad + \frac{\Omega_{r4}^2}{\Delta_4 + V}(-|00r\rangle\langle 00r| - |0r0\rangle\langle 0r0|\\
&\quad - |r00\rangle\langle r00| + |rr0\rangle\langle rr0|\\
&\quad + |r0r\rangle\langle r0r| + |0rr\rangle\langle 0rr|),
\end{aligned}
$$

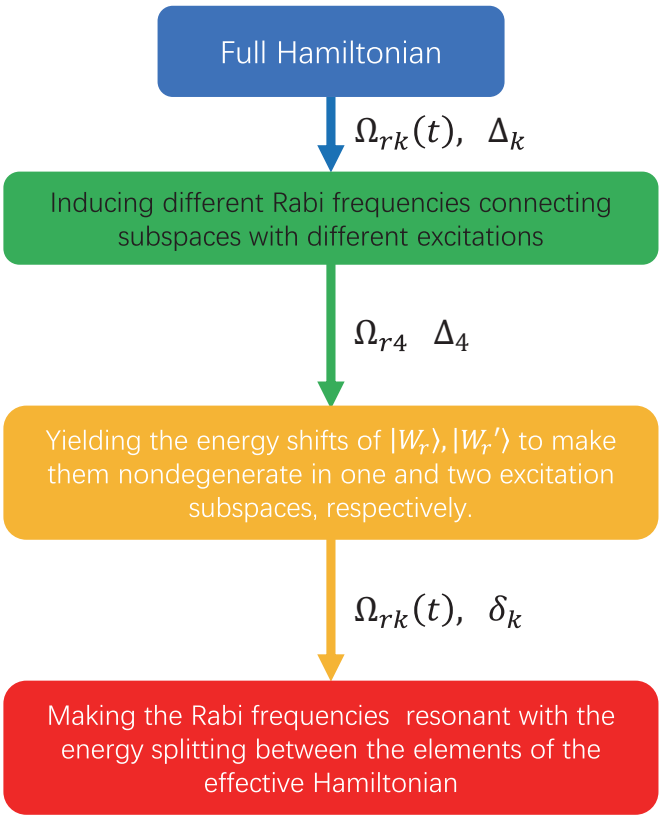

FIG. 10. Sketch map of deriving the effective Hamiltonian.

$$\begin{aligned} H_{e1i}(t) = {} & \sqrt{3}\Omega_{r1}(t)e^{i\delta_1 t}|000\rangle\langle W_r| \\ & + \sqrt{3}\Omega_{r3}(t)e^{i\delta_3 t}|W_r'\rangle\langle rrr| \\ & + \Omega_{r2}(t)e^{i\delta_2 t}(|00r\rangle\langle 0rr| + |00r\rangle\langle r0r| \\ & + |0r0\rangle\langle 0rr| + |0r0\rangle\langle rr0| \\ & + |r00\rangle\langle r0r| + |r00\rangle\langle rr0|) + \text{H.c.}, \end{aligned} \tag{A1}$$

with $|W_r\rangle = \frac{1}{\sqrt{3}}(|00r\rangle + |0r0\rangle + |r00\rangle)$ and $|W_r'\rangle = \frac{1}{\sqrt{3}}(|rr0\rangle + |r0r\rangle + |0rr\rangle)$. Here, H_{e10} is a time-independent Hamiltonian and much larger than the time-dependent Hamiltonian $H_{e1i}(t)$. Note that in Eq. (A1), $H_{e1i}(t)$ contains higher-order terms such as $2e^{-2i\delta_1 t}\Omega_{r1}(t)^2/V$, which have been neglected due to the condition $\{V,\ \Delta_4\} \gg \{\Omega_{r4},\ \delta_1,\ \delta_2,\ \delta_3\} \gg \max\{|\Omega_{r1}(t)|,\ |\Omega_{r2}(t)|,\ |\Omega_{r3}(t)|\}$.

We afterwards move into a rotating frame with respect to $e^{iH_{e10}t}$ and obtain

$$\begin{aligned} H_{e1i}'(t) = {} & \sqrt{3}\Omega_{r1}(t)e^{i\delta_1 t}e^{i\lambda_1 t}|000\rangle\langle W_r| \\ & + \sqrt{3}\Omega_{r3}(t)e^{i\delta_3 t}e^{i\lambda_2 t}|W_r'\rangle\langle rrr| \\ & + \Omega_{r2}(t)e^{i\delta_2 t}(e^{i\lambda_3 t} + 2e^{i\lambda_4 t})|W_r\rangle\langle W_r'| \\ & - \Omega_{r2}(t)e^{i\delta_2 t}e^{i\lambda_3 t}(|00r\rangle\langle rr0| + |0r0\rangle\langle r0r| \\ & + |r00\rangle\langle 0rr|) + \text{H.c.}, \end{aligned} \tag{A2}$$

with

$$\begin{aligned} \lambda_1 &= -\frac{6\Omega_{r4}^2}{\Delta_4} + \frac{4\Omega_{r4}^2}{\Delta_4 + V}, \quad \lambda_2 = \frac{4\Omega_{r4}^2}{\Delta_4 + V} - \frac{6\Omega_{r4}^2}{\Delta_4 + 2V}, \\ \lambda_3 &= -\frac{2\Omega_{r4}^2}{\Delta_4 + V}, \quad \lambda_4 = \frac{3\Omega_{r4}^2}{\Delta_4} - \frac{8\Omega_{r4}^2}{\Delta_4 + V} + \frac{3\Omega_{r4}^2}{\Delta_4 + 2V}. \end{aligned} \tag{A3}$$

Here we want to construct an effective Hamiltonian with a form such as $H_e(t) = \Omega_{e1}(t)|000\rangle\langle W_r| + \Omega_{e2}(t)|W_r\rangle\langle W_r'| + \Omega_{e1}(t)|W_r'\rangle\langle rrr| + \text{H.c.}$, which can be utilized to achieve the interconversions between the GHZ states and the W states. Hence, the values of δ_1, δ_2, and δ_3 should be adjusted to eliminate some unwanted terms in Eq. (A2), that is, choosing $\delta_1 = -\lambda_1$, $\delta_2 = -\lambda_4$, and $\delta_3 = -\lambda_2$, yielding

$$\begin{aligned} H_{e1i}(t)' = {} & \sqrt{3}\Omega_{r1}(t)|000\rangle\langle W_r| + \sqrt{3}\Omega_{r3}(t)|W_r'\rangle\langle rrr| \\ & + \Omega_{r2}(t)[e^{i(\lambda_3 - \lambda_4)t} + 2]|W_r\rangle\langle W_r'| \\ & - \Omega_{r2}(t)e^{i(\lambda_3 - \lambda_4)t}(|00r\rangle\langle rr0| \\ & + |0r0\rangle\langle r0r| + |r00\rangle\langle 0rr|) + \text{H.c.} \end{aligned} \tag{A4}$$

By exploiting the large detuning condition $\{\delta_1,\ \delta_2,\ \delta_3\} \gg \max\{|\Omega_{r1}(t)|,\ |\Omega_{r2}(t)|,\ |\Omega_{r3}(t)|\}$, i.e., $\{|\lambda_1|,\ |\lambda_4|,\ |\lambda_2|\} \gg \max\{|\Omega_{r1}(t)|,\ |\Omega_{r2}(t)|,\ |\Omega_{r3}(t)|\}$, the terms with high-frequency oscillations can be neglected and the effective Hamiltonian will be finally derived as

$$\begin{aligned} H_{\text{eff}}(t) = {} & \sqrt{3}\Omega_{r1}(t)|000\rangle\langle W_r| + \sqrt{3}\Omega_{r3}(t)|W_r'\rangle\langle rrr| \\ & + 2\Omega_{r2}(t)|W_r\rangle\langle W_r'| + \text{H.c.} \end{aligned} \tag{A5}$$

In a word, such a course of reducing the original Hamiltonian is shown in Fig. 10.

[1] D. P. Divincenzo, Science **270**, 255 (1995).
[2] C. H. Bennett, G. Brassard, C. Crepeau, R. Jozsa, A. Peres, and W. K. Wootters, Phys. Rev. Lett **70**, 1895 (1993).
[3] A. K. Ekert, Phys. Rev. Lett. **67**, 661 (1991).
[4] G. Gordon and G. Rigolin, Phys. Rev. A **73**, 042309 (2006).
[5] J. S. Bell, Physics **1**, 195 (1964).
[6] A. Cabello, Phys. Rev. A **65**, 032108 (2002).
[7] S. B. Zheng, Phys. Rev. A **66**, 014103 (2002).
[8] W. Dür, G. Vidal, and J. I. Cirac, Phys. Rev. A **62**, 062314 (2000).
[9] E. Jung, M. R. Hwang, Y. H. Ju, M. S. Kim, S. K. Yoo, H. Kim, D. K. Park, J. W. Son, S. Tamaryan, and S. K. Cha, Phys. Rev. A **78**, 012312 (2008).
[10] A. Karlsson and M. Bourennane, Phys. Rev. A **58**, 4394 (1998).
[11] J. Joo, Y. J. Park, S. Oh, and J. Kim, New J. Phys. **5**, 136 (2003).
[12] L. H. Jin, X. R. Jin, and S. Zhang, Phys. Rev. A **72**, 024305 (2005).
[13] T. Gao, F. L. Yan, and Z. X. Wang, J. Phys. A: Math. Gen. **38**, 5761 (2005).
[14] X. R. Jin, X. Ji, Y. Q. Zhang, S. Zhang, S. K. Hong, K. H. Yeon, and C. I. Um, Phys. Lett. A **354**, 67 (2006).

[15] A. M. Lance, T. Symul, W. P. Bowen, B. C. Sanders, and P. K. Lam, Phys. Rev. Lett. **92**, 177903 (2004).
[16] M. Hillery, V. Bužek, and A. Berthiaume, Phys. Rev. A **59**, 1829 (1999).
[17] P. Walther, K. J. Resch, and A. Zeilinger, Phys. Rev. Lett. **94**, 240501 (2005).
[18] T. Tashima, T. Wakatsuki, Ş. K. Özdemir, T. Yamamoto, M. Koashi, and N. Imoto, Phys. Rev. Lett. **102**, 130502 (2009).
[19] T. Tashima, M. S. Tame, Ş. K. Özdemir, F. Nori, M. Koashi, and H. Weinfurter, Phys. Rev. A **94**, 052309 (2016).
[20] W. X. Cui, S. Hu, H. F. Wang, A. D. Zhu, and S. Zhang, Opt. Express **24**, 15319 (2016).
[21] Y. H. Kang, Z. C. Shi, B. H. Huang, J. Song, and Y. Xia, Phys. Rev. A **100**, 012332 (2019).
[22] S. B. Zheng and G. C. Guo, Phys. Rev. Lett. **85**, 2392 (2000).
[23] S. B. Zheng, Phys. Rev. A **87**, 042318 (2013).
[24] Y. H. Chen, Y. Xia, Q. Q. Chen, and J. Song, Sci. Rep. **5**, 15616 (2015).
[25] Y. H. Chen, Z. C. Shi, J. Song, Y. Xia, and S. B. Zheng, Phys. Rev. A **97**, 032328 (2018).
[26] Y. H. Chen, Z. C. Shi, J. Song, and Y. Xia, Phys. Rev. A **97**, 023841 (2018).
[27] Y. H. Kang, Y. H. Chen, Z. C. Shi, B. H. Huang, J. Song, and Y. Xia, Phys. Rev. A **97**, 042336 (2018).
[28] R. H. Zheng, Y. H. Kang, Z. C. Shi, and Y. Xia, Ann. Phys. (Berlin) **530**, 1800133 (2018).
[29] Y. Wang, C. S. Hu, Z. C. Shi, B. H. Huang, J. Song, and Y. Xia, Ann. Phys. (Berlin) **531**, 1900006 (2019).
[30] S. Felicetti, M. Sanz, L. Lamata, G. Romero, G. Johansson, P. Delsing, and E. Solano, Phys. Rev. Lett. **113**, 093602 (2014).
[31] R. H. Zheng, Y. H. Kang, Z. C. Shi, and Y. Xia, Ann. Phys. (Berlin) **531**, 1800447 (2019).
[32] L. Garziano, V. Macrí, R. Stassi, O. Di Stefano, F. Nori, and S. Savasta, Phys. Rev. Lett. **117**, 043601 (2016).
[33] S. Liu, D. Ran, Z. C. Shi, J. Song, and Y. Xia, Ann. Phys. (Berlin) **531**, 1900086 (2019).
[34] J. Song, X. D. Sun, Q. X. Mu, L. L. Zhang, Y. Xia, and H. S. Song, Phys. Rev. A **88**, 024305 (2013).
[35] G. Y. Wang, D. Y. Wang, W. X. Cui, H. F. Wang, A. D. Zhu, and S. Zhang, J. Phys. B **49**, 065501 (2016).
[36] D. Jaksch, J. I. Cirac, P. Zoller, S. L. Rolston, R. Côté, and M. D. Lukin, Phys. Rev. Lett. **85**, 2208 (2000).
[37] E. Urban, T. A. Johnson, T. Henage, L. Isenhower, D. D. Yavuz, T. G. Walker, and M. Saffman, Nat. Phys. **5**, 110 (2009).
[38] C. Ates, T. Pohl, T. Pattard, and J. M. Rost, Phys. Rev. Lett. **98**, 023002 (2007).
[39] X. Q. Shao, J. H. Wu, X. X. Yi, and Gui-Lu Long, Phys. Rev. A **96**, 062315 (2017).
[40] E. Torrontegui, S. Martínez-Garaot, and J. G. Muga, Phys. Rev. A **89**, 043408 (2014).
[41] H. R. Lewis and W. B. Riesenfeld, J. Math. Phys. **10**, 1458 (1969).
[42] I. Medina and F. L. Semião, Phys. Rev. A **100**, 012103 (2019).
[43] T. Wilk, A. Gaëtan, C. Evellin, J. Wolters, Y. Miroshnychenko, P. Grangier, and A. Browaeys, Phys. Rev. Lett. **104**, 010502 (2010).
[44] S. L. Su, Y. Z. Tian, H. Z. Shen, H. P. Zang, E. J. Liang, and S. Zhang, Phys. Rev. A **96**, 042335 (2017).
[45] M. J. Hartmann, F. G. S. L. Brandão, and M. B. Plenio, Nat. Phys. **2**, 849 (2006).
[46] J. D. Pritchard, D. Maxwell, A. Gauguet, K. J. Weatherill, M. P. A. Jones, and C. S. Adams, Phys. Rev. Lett. **105**, 193603 (2010).
[47] A. Omran, H. Levine, A. Keesling, G. Semeghini, T. T. Wang, S. Ebadi, H. Bernien, A. S. Zibrov, H. Pichler, S. Choi, J. Cui, M. Rossignolo, P. Rembold, S. Montangero, T. Calarco, M. Endres, M. Greiner, V. Vuletić, and M. D. Lukin, Science **365**, 570 (2019).
[48] C. Song, K. Xu, H. Li, Y. Zhang, X. Zhang, W. Liu, Q. Guo, Z. Wang, W. Ren, J. Hao, H. Feng, H. Fan, D. Zheng, D. Wang, H. Wang, and S. Zhu, Science **365**, 574 (2019).
[49] X. F. Shi, Phys. Rev. Appl. **11**, 044035 (2019).